Prediction of the Effect of Vortex Generators on Airfoil Performance

Sørensen, Niels N.; Zahle, Frederik; Bak, Christian; Vronsky, T.

Published in:
Journal of Physics: Conference Series (Online)

Link to article, DOI:
10.1088/1742-6596/524/1/012019

Publication date:
2014

Document Version
Publisher's PDF, also known as Version of record

Prediction of the Effect of Vortex Generators on Airfoil Performance

2014 J. Phys.: Conf. Ser. 524 012019

(http://iopscience.iop.org/1742-6596/524/1/012019)

Prediction of the Effect of Vortex Generators on Airfoil Performance

Niels N. Sørensen[1], **F. Zahle**[1], **C. Bak**[1], **T. Vronsky**[2]

[1] Technical University of Denmark, Department of Wind Energy, Risø Campus, Frederiksborgvej 399, 4000 Roskilde Denmark
[2] Vestas Wind Systems A/S

E-mail: nsqr@dtu.dk

Abstract. Vortex Generators (VGs) are widely used by the wind turbine industry, to control the flow over blade sections. The present work describes a computational fluid dynamic procedure that can handle a geometrical resolved VG on an airfoil section. After describing the method, it is applied to two different airfoils at a Reynolds number of 3 million, the FFA-W3-301 and FFA-W3-360, respectively. The computations are compared with wind tunnel measurements from the Stuttgart Laminar Wind Tunnel with respect to lift and drag variation as function of angle of attack. Even though the method does not exactly capture the measured performance, it can be used to compare different VG setups qualitatively with respect to chord-wise position, inter and intra-spacing and inclination of the VGs already in the design phase.

1. Introduction

In the wind turbine industry VGs are a widely used device to control the flow over parts of the blades. The application of VGs to limit flow separation has a long history, originating from the work of Taylor [15] where vane type VGs were applied to limit flow separation. In connection with wind energy applications one of the early references is the work on the Mod-2 wind turbine by Sullivan [13] where an 11 percent increase in annual energy production was reported.

From an engineering point of view, there is a strong need for knowledge on how to incorporate VGs into the design process at an early stage in order to choose the size, shape, position and inclination angles of the VGs. In the design codes used by industry all that is needed to do this is the lift, drag and moment polars for the airfoil sections equipped with VGs.

The standard way to obtain this is through wind tunnel experiments which can be costly and also difficult to perform at the high Reynolds numbers needed today and for the relatively thick airfoils sections typically used on modern blades.

An alternative or supplementary approach to the direct experimental approach is to use e.g. Navier-Stokes based CFD tools to directly compute the effects of VGs during the design phase.

Due to the large range of scales present for a wing equipped with VGs, it is not computationally feasible to directly attack the problem using a full wind turbine blade equipped with a large number of VGs (typically in the order of hundreds of VGs). Two approaches have typically been applied, either using a model for the VG, either in the form of inserting volume forces as in the BAY type of models, Bender [1], Perivolaris [10], or by modeling the boundary layer mixing effect of the VG by increasing the turbulence kinetic energy at the VG position

Hansen et al. [3]. Avoiding the need to resolve the boundary layer on the actual VGs makes it possible to actually model the full physical configuration, see Tai [14].

When directly representing the VG in the computation by resolving the geometry, and thereby avoiding the need for additional modeling, often simpler problems are addressed, either VGs on flat plates, Fernandez [2] or span-wise periodic airfoil sections see Joubert [4].

2. Numerical study

The DTU Wind Energy flow solver EllipSys3D is used in all computations presented in this paper. The code is developed in co-operation between the former Department of Mechanical Engineering at the Technical University of Denmark and the former Department of Wind Energy at Risø National Laboratory, Risø-DTU, see Michelsen [8, 9] and Sørensen [11].

In the present work the turbulence in the boundary layer is modeled by the k-ω Shear Stress Transport (SST) eddy viscosity model Menter [6]. The effects of laminar/turbulent transition in the boundary layer on the blade is modeled with the $\gamma - \widetilde{\mathrm{Re}}_\theta$ correlation based transition model of Menter [7], for the present implementation see Sørensen [12].

In the present simulations, the EllipSys3D code is used in steady state mode, running local time stepping towards a steady state solution. The diffusive terms are discretized with a second order central differencing scheme. The convective fluxes are computed using the third order accurate QUICK scheme of Leonard [5], both for the momentum, turbulence equations, and the equations of the transition model. For all simulations the convergence criteria is a reduction of the residual by a factor of 100.000.

3. Vortex Generator Setup

The VG configurations investigated in the present work are all in a counter rotating configuration as seen in Figure 1. In order to limit the computational requirements, only one of the two vanes in a VG unit is simulated exploiting the geometrical symmetry of a VG unit. The parameters characterizing the VG configuration are: the size, the aspect ratio of the delta wings, the angles of the delta wings with the oncoming flow, and the inter and intra spacing of the VG units, see Figure 1. For all cases studied here the height (h) of the VG is 1 percent of the chord length, the aspect ratio (l/h) of the VG is approximately 3.8 and the inclination with the incoming flow (β) is 15.5 degrees, the distance between the VG within the pairs is $\Delta 1/h \sim 5$ at the leading edge of the VG, while the distance at the leading edge to the next VG pair is $\Delta 2/h \sim 4$

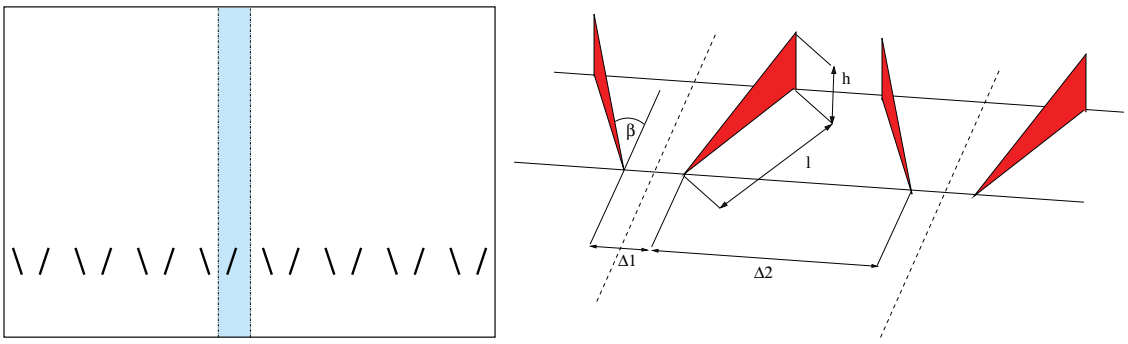

Figure 1. The left side of the figure shows a sketch of a top-down view of an airfoil with the leading edge toward the bottom equipped with VGs. The colored region indicates the symmetry unit used in the computations. The right side of the figure shows an non-scalable sketch defining the characteristic dimensions of the VG setup.

To justify the symmetry assumption used in the present computations, the behavior of the trailed vorticity behind VGs positioned at x/C=0.30 is compared with the limiting streamlines on the suction side of the airfoil from the experient in the Stuttgart Laminar Wind Tunnel, see Figure 2. Even though the present mesh is not conserving a very distinct vortex structure near the trailing edge of the airfoil the vortex structure is still clearly visible. Grid refinement studies have shown that preserving the vortex structure all the way to the trailing edge is a prerequisite for obtaining the VG effect on the airfoil.

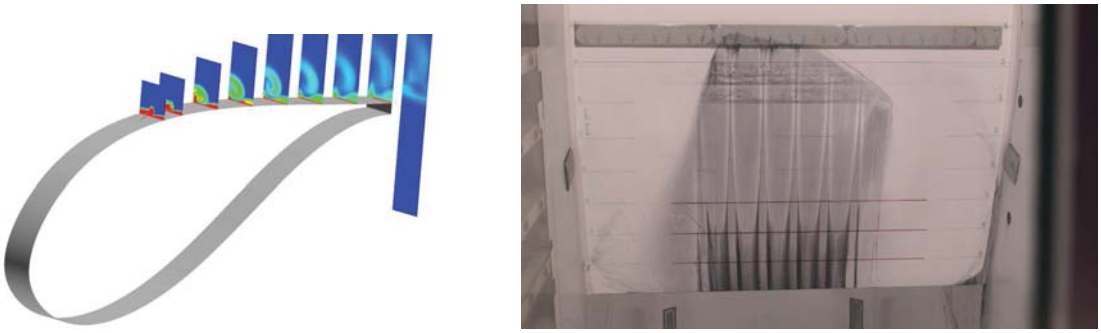

Figure 2. The left picture shows the computed vortex trailed behind the VG placed at $x/C = 30$ percent on the suction side of the FFA-W3-301, the vortex structure is visible all the way to the trailing edge even though diffusion is slowly smearing the structure. The right picture shows the food print of the vortex for a similar situation in the Stuttgart Laminar Wind Tunnel, curtesy of Stuttgart [16].

4. Grid Generation

In order to allow systematic studies of the effect of delta shaped VGs on the airfoil performance, it is crucial that parametric studies can be performed. This requires efficient grid generation that allows easy variation of the VG setup. The main parameters of interest in this connection is the chord-wise position of the VGs, the size of the VG, the aspect ratio of the VG, the inclination of the VG and the inter and intra spacing of the VG pairs. To limit the necessary effort to generate the computational grids, the grid generation is split in several sub-processes. First, a surface grid is generated for half a VG unit, fixing the size, aspect ratio, inclination and the inter and intra spacing of the VG pairs, see Figure 3. This part of the grid generation is done in the commercial grid generator called Pointwise. For a given aspect ratio of the delta shaped VG, it is relatively easy to change the size, inclination, and inter and intra spacing of the VG pairs. The present methodology allows a library of different VG setups to be made and reused on different airfoils highly reducing the grid generation time.

Having generated the desired VG unit, it can be combined with an arbitrary 2D airfoil shape and positioned at a specific chord-wise position by running a small program distributing the grid points around the airfoil geometry, see Figure 4.

Finally, the volume grid can be generated using the in-house hyperbolic grid generator HypGrid3D by simply marching the grid normal to the airfoil surface, see Figure 5. One consequence of the block structured topology is that all grid cells from the VG unit will be carried all the way to the far-field. Here the cells due to the limited expansion possible in the span- and chord-wise direction will result in high aspect ratio cells. To avoid excessive grid generation problems, the distance to the far-field boundary is relaxed from the normal 30-40 to 16 chord lengths.

The 3D grids are generated based on the knowledge from previous 2D and 3D airfoil computations with a y^+ value below 2 everywhere on the airfoil, a chordwise resolution of 389 cells, a spanwise resolution of 64 cells and normal resolution of 128 cells. The effect of coarsening the grid by a factor of two in all direction is included in Figure 10 which clearly shows that the stall angle is influenced by the resolution while the results below the predicted stall angle is grid independent. This indicates that higher grid resolution might be needed to accurately capture the stall onset, but this is left to later studies. Here, the focus is mainly on illustrating the overall possibilities of the method.

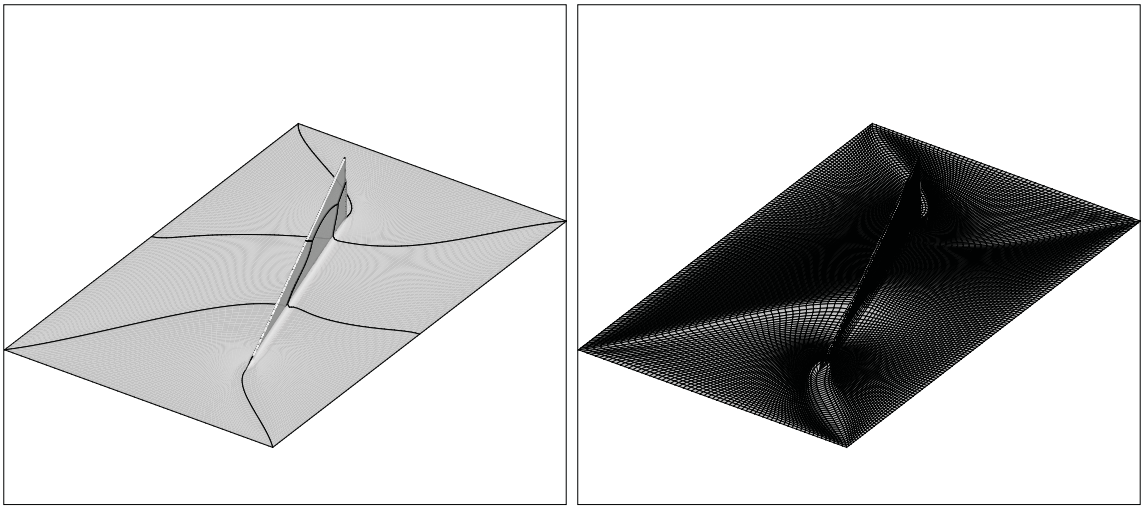

Figure 3. An example of a VG unit used for the airfoil simulations. The left picture shows the VG surface with the block structure around the VG and the right picture shows the surface grid on the VG unit.

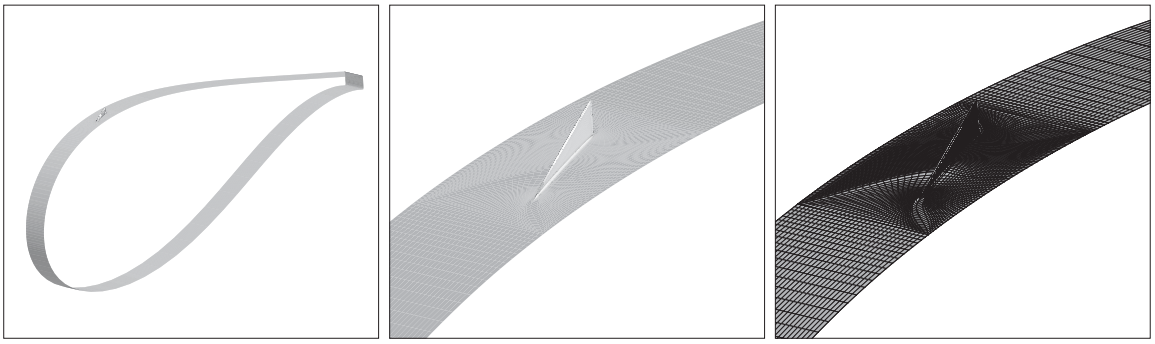

Figure 4. A VG unit positioned on the airfoil geometry. The pictures show from left to right: overview of the VG on the airfoil geometry, close-up of the VG, and the block structure of the grid around the VG.

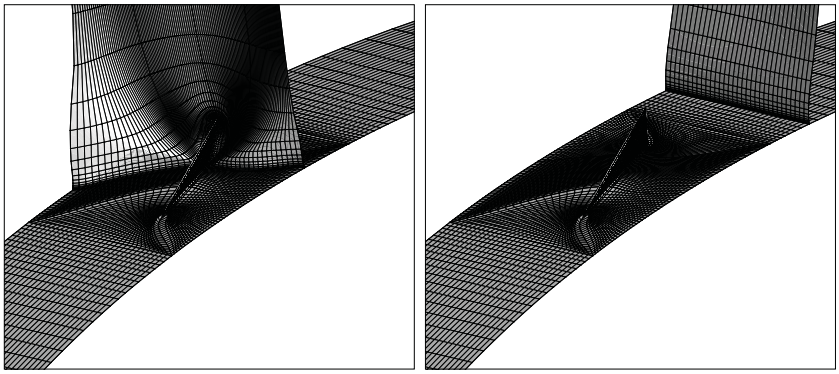

Figure 5. Grid structure around the VG positioned on the airfoil, here only showing every second grid point. The pictures show in the left picture the grid wrapping around the delta wing shape, and in the right picture a grid plane downstream of the VG.

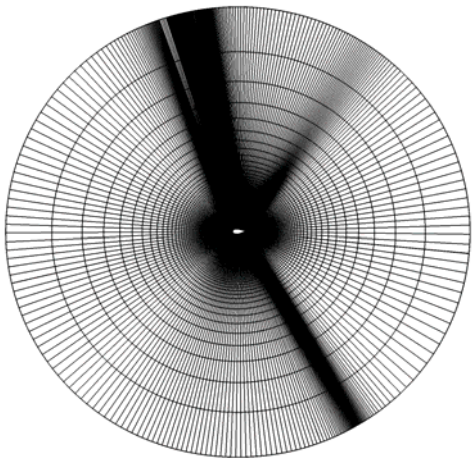

Figure 6. A span-wise cut through the grid topology showing a typical 2D O-mesh structure. Due to the block structured topology, the grid cells from the VG unit will develop high aspect ratios in the far-field and prevents that the outer boundary of the grid can be placed at the normal distance of 30-40 chord length.

5. Results

5.1. Preliminary Test

Before starting the actual investigation, a crude study is performed of the effect of the limited distance to the far-field location where the undisturbed velocity is specified, to clarify if the close proximity of the farfield boundary will influence the solution. A 2D study is performed for the clean airfoil configuration in fully turbulent conditions showing a minimal interference when varying the distance from $\sim$ 32 chords to $\sim$ 16 chords, see Figure 7. From the figure it is evident that untill stall difference between the results on the two domain sizes is negligible, and even in stall, the difference is small. Additionally, as all configuration are computed on a similar grid setup, it is believed that the present setup will allow a good relative comparison of the different VG configurations.

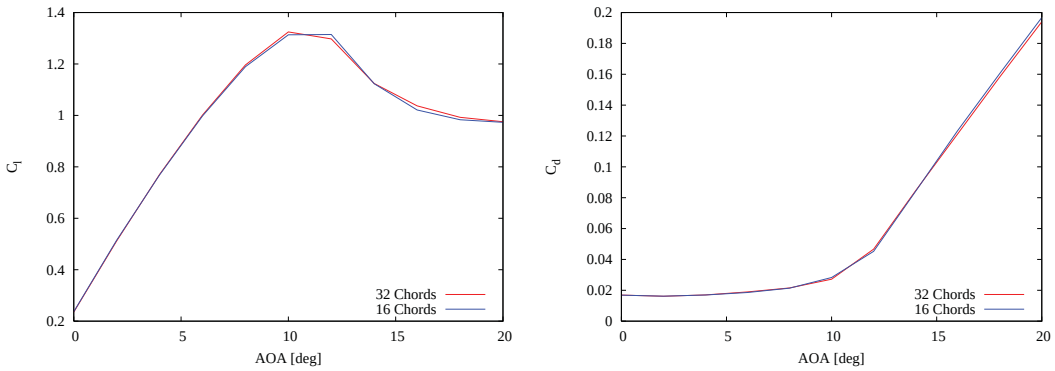

Figure 7. Comparison of the 2D airfoil computations performed on a domain with the far-field placed 16 and 32 chords from the airfoil surface, for the FFA-W3-301 airfoil at a Reynolds number of 3 million.

5.2. FFA-W3-301 Airfoil

Three configurations of the 30 percent thick FFA-W3-301 airfoil were investigated, with the VG unit placed with its leading edge at $x/C \sim 0.15$, $x/C \sim 0.20$ and $x/C \sim 0.30$, respectively. The Reynolds number for all simulations were 3 million based on the airfoil chord and the free stream velocity. The computations are compared to experimental data taken in the Stuttgart wind tunnel, Würz et al. [16], for the cases where data are available.

When comparing the lift and drag between measurements and computations, it must be remembered that the VG modeled in the computations is idealized compared to the actual one used in the measurements. In the measurements the VGs are equipped with a rather substantial base plate to help with the positioning and alignment. Unfortunately more recent experiments have revealed that the VG base generate nearly one third of the drag increase observed in the measurements, and additionally, the base plate has the effect of decreasing the lift similar to adding roughness to the leading edge. Furthermore, with respect to the computations it must be expected that including the VG configuration in the 3D CFD computations will not circumvent the well established problem of the CFD RANS method of predicting the excact stall onset angle and the performance in stalled conditions.

The overall tendency of the computations can be observed by comparison of Figures 8 to 10 where the lift and drag are shown for the three configurations.

Starting by comparing the cases with the VG positioned at 15 percent chord (where only computations exist) with the cases with the VG at the 20 percent chordwise position, a one degree delay in the stalling angle can be observed when the VG is moved towards the leading edge, see Figure 8. In agrement with other experimental observations the delay in stall angle when moving the VG towards the leading edge is accompanied by a decreased lift slope close to stall onset. The price paid for the increased stalling angle is observed in the right hand side of Figure 8, showing an increase in drag when moving the VG towards the leading edge. Compared to the clean configuration both the computed configurations have improved lift performance at the price of some additional drag at the lower angles of attack.

For the 20 and 30 percent cases where measurements exist for both cases, a similar tendency of the lift variations with VG position is observed in both experiment and measurements, namely an increased delay in stall angle accompanied by a decreasing lift slope close to stall when moving the VG towards the leading edge. For this case, even though the lift slope decreased the accompanied delayed in stall angle dictates a higher C_l max when positioning the VG closer to the leading edge (x/C=0.20), see Figure 9 and 10.

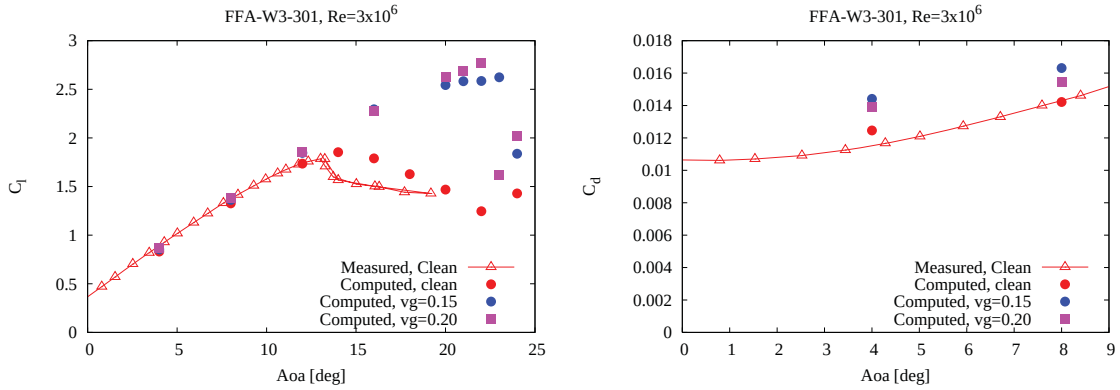

Figure 8. Comparison of computed setup with the VG at x/C=0.15 and x/C=0.20 with measured lift and drag for the clean FFA-W3-301 airfoil at a Reynolds number of 3 million.

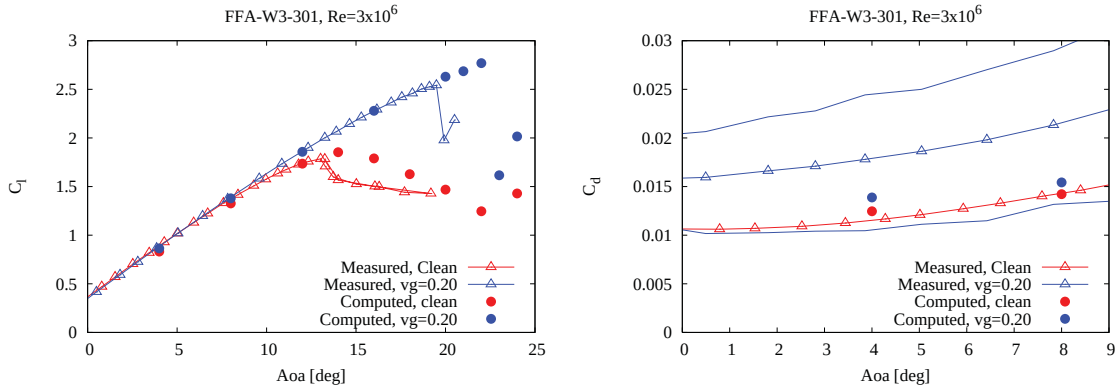

Figure 9. Comparison of computed and measured lift and drag for the FFA-W3-301 airfoil at a Reynolds number of 3 million, with the VG placed at x/C=0.20. For the measured drag the min and max value of the spanwise sinusoidaely varying drag are shown with lines only.

Looking at the drag in the experimental data, Figure 9 and Figure 10, three different drag curves are available from the wake deficit measurements, namely the span-wise mean value indicated with both line and symbols, the minimum and maximum drag observed along the span indicated only with lines. While the three curves are nearly identical for the clean airfoil (not shown here), the fact that the drag varies sinusoidalely along the span depending on whether the drag is determined from the wake directly behind a VG or from the wake behind the free space between these, introduces the much higher drag variation for the VG cases.

Comparing the drag in Figures 8 to 10, the picture is not quite as clear as for the lift. First of all the increase in the mean drag in the computations is much smaller than the observed drag increase in the experiment. Even when subtracting approximately on third of the drag that has recently been shown to be attributed to the base plate, the computations seem overly optimistic with respect to the drag prediction. This being said, the computations are still able to capture the qualitative effect of increasing drag at low AOA's for all configuration.

Finally, a more detailed study of the pressure distributions for the FFA-W3-301 airfoil is shown for three configurations, clean, VG at 20 percent chord and VG at 30 percent chord at

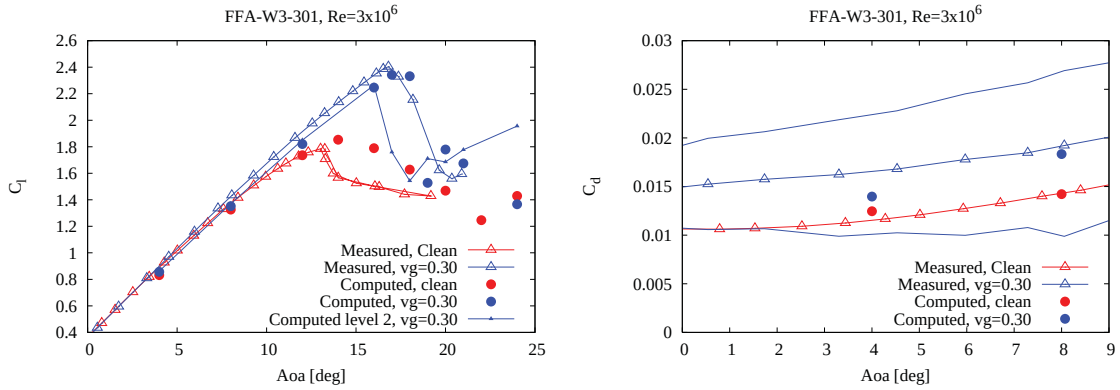

Figure 10. Comparison of computed and measured lift and drag for the FFA-W3-301 airfoil at a Reynolds number of 3 million, with the VG placed at x/C=0.30. For the measured drag the min and max value of the spanwise sinusoidaely varying drag are shown with lines only.

four different angles of attack $\sim$ [4, 8, 16, 20] degrees, see Figure 11. The pressure contours are extracted at 10 cross sections accross the span, resulting in several sections intersecting the actual VG position producing the wiggles like structure present in Figure 11. Additionally, this representation also illustrates that the computed flow remains steady and with a 2D like behaviour on the remaining part of the airfoil. In the figures the measured and the computed angles of attack do not agree fully and some deviation might be observed due to this. Additionally, even though the experimental lift and drag values are corrected using wind tunnel corrections as described in Würz et al. [16], the correction to the pressure distribution is not a simple shift of the angle of attack and is therefore not included.

Even though the agreement is not perfect it is observed that at the lower angles of attack 4 and 8 degrees, the pressure distributions are similar for all three configurations. When the clean airfoil is starting to separate at 16 degrees, the two VG configurations preserve attached flow in both simulations and measurements. The good qualitative agreement of the computed and measured pressure distribution for the two VG configuration indicates that the computations are capturing the right physics.

At the highest angle of attack of 20 degrees, no measurements are taken for the clean configuration, while both the measured VG configurations are heavily stalled, see Figure 11. From Figure 9 it is clear that stall is taking place right around $\sim$ 20 degrees for the computed x/C=0.20 configuration, while Figure 10 shows that stall is happening already around $\sim$ 18 degrees for the computed x/C=0.30 configuration.

5.3. FFA-W3-360

The 36 percent thick FFA-W3-360 is also investigated, and among the experimental tested setups we concentrate on the configurations with VGs placed at $x/C \sim 0.15$ and $x/C \sim 0.20$ from the leading edge in the computations. The Reynolds number for all simulations and measurements is 3 million based on the airfoil chord and the free stream velocity. The computations are again compared to experimental data taken in the Stuttgart Laminar Wind Tunnel, Würz et al. [16].

Looking at Figure 12 the first obvious observation is that for the 36 percent thick airfoil the agreement of the lift slope between computations and measurements below C_l max is not capture in contrast to observations for the thinner 30 percent airfoil. The recent observation that the VG baseplate can have an effect similar to leading edge roughness together with the knowledge that roughness typically has a strong effect on thick airfoils, making the airfoil lift slope non-linear

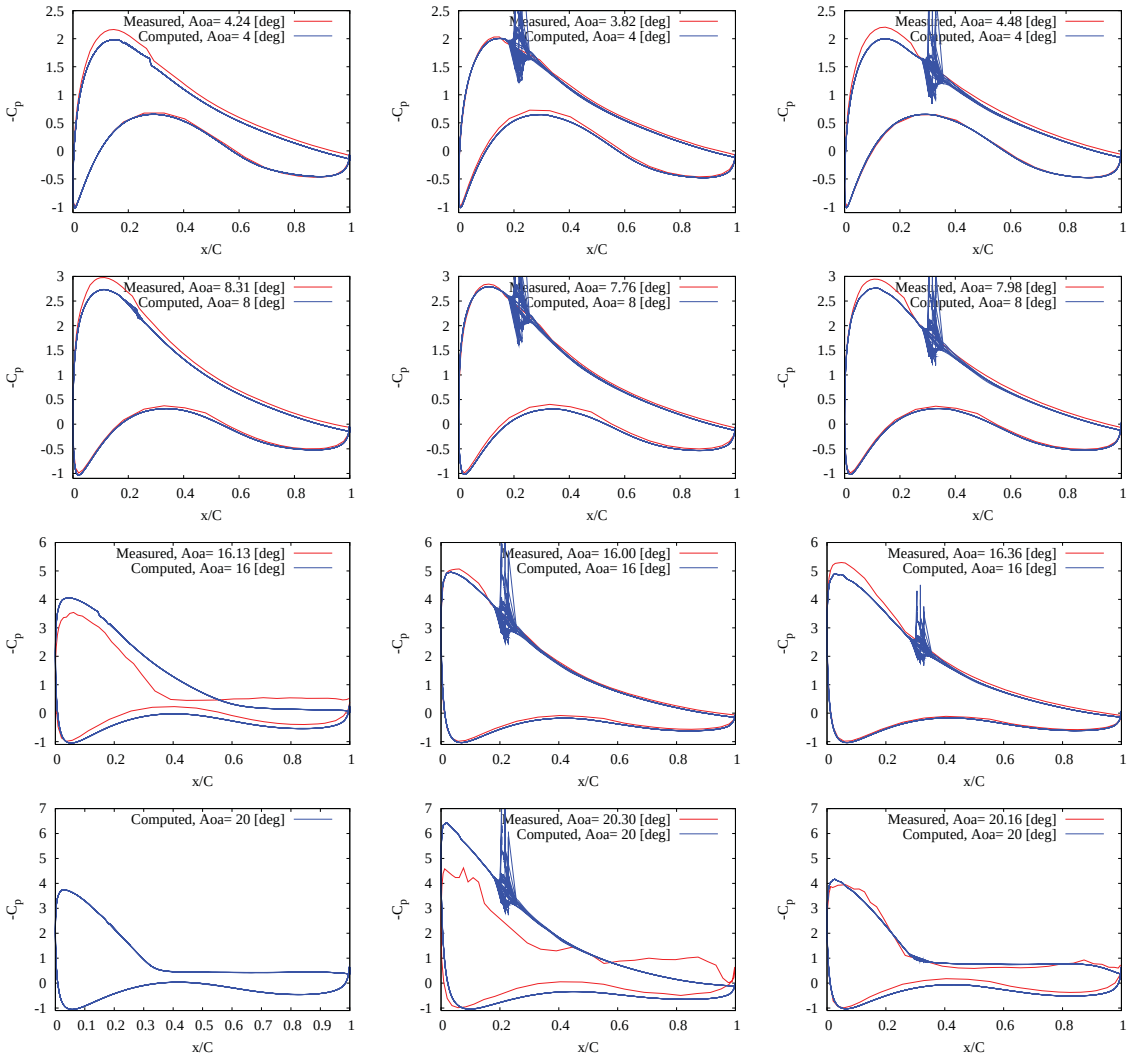

Figure 11. Comparison of computed and measured pressure distributions for the FFA-W3-301 airfoil at a Reynolds number of 3 million, for a clean airfoil left, a VG placed at x/C=0.20 center and a VG placed at x/C=0.30 right column.

below stall could be one obvious explanation. This is supported by the fact that the lift slope is greatly improved in the measurements by moving the VG towards the trailing edge from 0.15 to 0.20 percent. Additionally, the agreement between the measured and computed configuration with the VG at 20 percent is clearly improved compared to the 15 percent configuration, see Figur 12.

It is hypothesized that the destructive effect of the baseplate compared to the beneficial effect of the VG is dominating for the configuration with the VG at $x/C \sim 0.15$. When moving the VG towards the trailing edge, resulting in a larger ratio between boundary layer and baseplate height, the beneficial effect of the VG starts to dominate in the region between 10 and 16 degrees angle of attack . This is observed in the measurements by the recovery of a linear lift slope up to 16 degrees. For higher angles of attack the deviation is proably due to the well know

shortcomming of RANS CFD to predict the onset and deep stall behaviour.

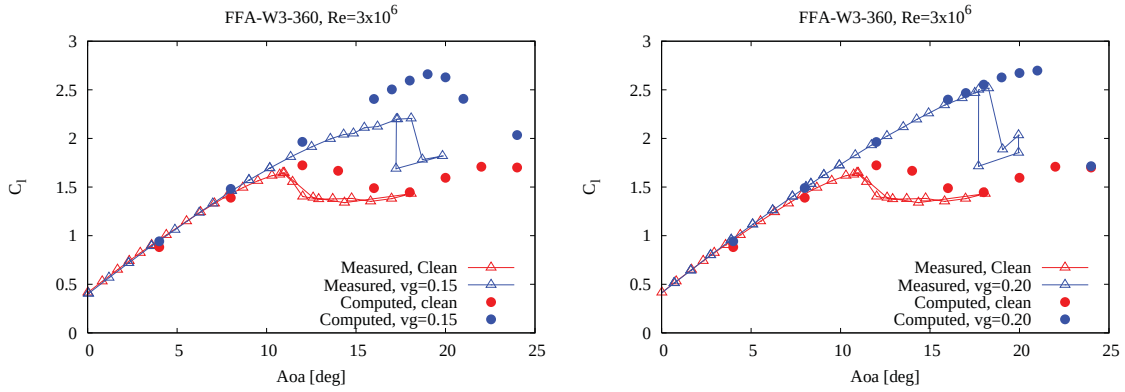

Figure 12. Comparison of computed and measured lift for the FFA-W3-360 airfoil at a Reynolds number of 3 million, with the VG placed at x/C=0.15.

6. Conclusion and future work

This paper describes a methodology for computing the effect of Vortex Generators on airfoil sections using Computation Fluid Dynamics. A grid generation method is developed that allows easy repositioning of the VG in chord-wise direction on different airfoil sections, and where other VG parameters like inter- and intra-spacing and the inclination angle can relatively easy be changed and stored in a library of VG units. It is shown that the method is in fact capable of predicting the qualitative effect of VGs and even though the method fails to predict the excact stall onset angle it captures the lift in the extended attached region well. It is demonstrated that the method is a large improvement to typical CFD approach where VG are simply neglected in the computations and that the method can be used to qualitatively compare different VG setups. Some complications compared to the measurements are described, mainly the roughness like effect of the relatively large base plate of the present VGs, and future computational studies are planned where the VG base is included in the computations. The high degree of details provided by the CFD simulations can directly be used to investigate many of the boundary layer changes generated by the VGs. Additionally, the load characteristics can be extracted from the present type simulations and used in simpler models or BAY type CFD models.

7. Acknowledgement

The present investigation was funded from the project Light Rotor, EUDP 64010-0107, while the development of the computational procedure took place in the project Optimization of vortex generators on wind turbine blades, EUDP 64009-0279. Computation was made possible by the use of GORM PC-cluster at the DTU central computing facility at DTU Risø Campus.

8. References

[1] E. E. Bender, P. J. Yagle, and B. H. Anderson. Vortex generator modeling for navier-stokes codes. *Proceedings of the 1999 3rd ASME/JSME Joint Fluids Engineering Conference, FEDSM'99, San Francisco, California, USA, 18-23 July 1999 (CD-ROM)*, pages 1–, 1999.

[2] U. Fernandez, Pierre-Elouan Rethore, Niels N. Sørensen, Clara Marika Velte, Frederik Zahle, and E. Egusquiza. Comparison of four different models of vortex generators. *Proceedings of EWEA 2012 - European Wind Energy Conference & Exhibition*, 2012.

[3] M. O. L. Hansen and C. Westergaard. Phenomenological model of vortex generators. *AERODYNAMICS OF WIND TURBINES -SYMPOSIUM-*, pages 1–8, 1995.
[4] G. Joubert, A. Le Pape, B. Heine, and S. Huberson. Vortical interactions behind deployable vortex generator for airfoil static stall control. *AIAA JOURNAL*, 51(1):240–252, 2013.
[5] B. P. Leonard. A stable and accurate convective modelling procedure based on quadratic upstream interpolation. *Comput. Meths. Appl. Mech. Eng.*, 19:59–98, 1979.
[6] F. R. Menter. Zonal Two Equation k-ω Turbulence Models for Aerodynamic Flows. *AIAA paper 1993-2906*, 1993.
[7] F. R. Menter, R. B. Langtry, S. R. Likki, Y. B. Suzen, P. G. Huang, and S. Völker. A Correlation-Based Transition Model Using Local Variables, Part I - Model Formulation. In *Proceedings of ASME Turbo Expo 2004, Power for Land, Sea, and Air*, Vienna, Austria, June 14-17 2004. ASME. GT2004-53452.
[8] J. A. Michelsen. Basis3D - a Platform for Development of Multiblock PDE Solvers. Technical Report AFM 92-05, Technical University of Denmark, Department of Fluid Mechanics, Technical University of Denmark, December 1992.
[9] J. A. Michelsen. Block structured Multigrid solution of 2D and 3D elliptic PDE's. Technical Report AFM 94-06, Technical University of Denmark, Department of Fluid Mechanics, Technical University of Denmark, May 1994.
[10] Y. G. Perivolaris and S. G. Voutsinas. A cfd performance analysis of vortex generators used for boundary layer control on wind turbine blades. *EWEC -CONFERENCE-*, pages 522–525, 2001.
[11] N. N. Sørensen. General Purpose Flow Solver Applied to Flow over Hills. Risø-R- 827-(EN), Risø National Laboratory, Roskilde, Denmark, June 1995.
[12] Niels N. Sørensen. Cfd modelling of laminar-turbulent transition for airfoils and rotors using the $\gamma - \tilde{Re}_\theta$ model. *Wind Energy*, 12(8):715–733, 2009.
[13] Timothy L. Sullivan. Effect of vortex generators on the power conversion performance and structural dynamic loads of the mod-2 wind turbine. *NASA Technical Memorandum*, 1984.
[14] T. Tai. Effect of micro-vortex generators on v-22 aircraft forward-flight aerodynamics. In *40th AIAA Aerospace Sciences Meeting & Exhibit*, Aerospace Sciences Meetings. American Institute of Aeronautics and Astronautics, 2002.
[15] H.D. Taylor. Increasing the efficiency of the u.a.c. 8-ft wind tunnel fan by means of vortex generators. Technical Report R-4012-4, U.A.C., November 1947.
[16] W. Würz, B. Plogmann, C. Vetter, and M. Langohr-Kolb. Wind tunnel measurements of the ffa-w3-301 and ffa-w3-360 airfoils with vortx generators and gurney flaps. Technical report, Universität Stuttgart, Institut Für Aerodynamik Und Gasdynamik, IAG, February 2013.